Integrated sensing technologies for detection and location of leaks in water distribution networks

Alaa Hawari, Mohammad Khader, Walaa Hirzallah, Tarek Zayed and Osama Moselhi

ABSTRACT

Water distribution networks (WDNs) are infrastructure systems that have high socioeconomic values, for which efficient operation and management are required to ensure minimal amounts of waste which can be represented in the form of leaks. Leak detection is considered as one of the challenges faced by municipalities operating WDNs because it either involves shutting down the system or requires using expensive equipment and technologies. In this paper, a novel noninvasive and nondestructive methodology for detecting leaks in water pipes was tested. Ground penetrating radar was used for accurate determination of pipe location, followed by infrared (IR) thermographic imaging for determining the leak location using four different operating conditions. Results were statistically analyzed using analysis of variance and pairwise comparison methods. Several factors were found to affect the accuracy of the proposed methodology in predicting the leak location, namely, the characteristics of the studied surface (i.e. emissivity), the characteristics of the surrounding environment (i.e. ambient temperature and relative humidity), and the operating conditions of the IR camera (i.e. speed and height of the camera). The results obtained in this study have also shown that under high ambient temperatures and high relative humidity conditions, a higher speed of the IR camera would reduce the impact of noise on the collected thermal contrast and therefore, would give better leak location prediction results. The tested methodology proved the flexibility of the approach and the ability of accurately predicting the leak locations under different conditions.

Key words | ground penetrating radar, non-destructive, thermography, water leakage, water pipelines

Alaa Hawari (corresponding author)
Mohammad Khader
Walaa Hirzallah
Department of Civil and Architectural Engineering,
Qatar University,
P.O. Box 2713,
Doha,
Qatar
E-mail: *a.hawari@qu.edu.qa*

Tarek Zayed
Osama Moselhi
Department of Building Civil and Environmental Engineering,
Concordia University,
Montreal,
QC,
Canada

INTRODUCTION

Water distribution networks (WDNs) are considered to be one of the most valuable and crucial municipal infrastructure systems. They constitute the core of urban population growth, public health, welfare and safety (Cataldo *et al.* 2014). Nevertheless, according to a 2006 World Bank report, water losses through WDN were summed up to 45 million cubic metres daily in developing countries and more than 32 billion cubic metres annually on the global level (Kingdom *et al.* 2006). Water losses in the network do not only mean the loss of an invaluable resource, but also the loss of money spent on treating and transporting it and consequently the deterioration of the subterranean infrastructure (Ishido & Takahashi 2014; Xu *et al.* 2014). With significant population growth and subsequent increase in population density, the amount of stress on WDNs has increased and the risk of decreasing their lifetime and potential leaks have become much higher. Water leakage is a primary sign of pipe deficiency; therefore, monitoring the

doi: 10.2166/ws.2017.044

network and promptly detecting leaks is essential for its longevity and for the reduction of water losses (Alkasseh *et al.* 2013).

Various methods have been used in order to detect leaks in water networks. Leak detection can be classified into external and internal methods. In the external methods, signals are gathered outside the pipelines to detect leakage, whereas in internal methods signals are gathered inside the pipeline body to detect leakage. Visual inspection and thermographic methods are examples of the internal leak detection methods, while wave propagation is considered as an example of the external leak detection methods. Many of the common techniques currently used are to perturb the subsurface network either through shutting it down or through actual excavation and penetration. In addition, some of the common techniques used are flow and pressure monitoring, noise monitoring, visual inspection, electromagnetic techniques, and ultrasound techniques (Zangenehmadar & Moselhi 2014). Techniques that monitor the flow and pressure across the pipe can provide accurate results; however, to be able to obtain data that will be representative of the actual situation, monitoring over a long period of time is needed (Sun & Chang 2014; Zangenehmadar & Moselhi 2014). Therefore, these techniques are considered to be very time-intensive and are not applicable for immediate leak detections.

One of the methods that monitor the flow and pressure across the pipelines from which leak locations can be detected is negative pressure waves, used to detect leak locations in long pipelines conveying liquids (Ge *et al.* 2008). In this method different mathematical formulae are used to calculate the attenuation of negative pressure waves in the pipelines from which the leak flow can be calculated (Huang *et al.* 2007). This method is considered simple, low in cost and the results obtained for the leak locations are found to be satisfactory, however it is not appropriate for short pipelines. Another similar technique is called the 'fiber sensor based leak detection method' in which optical sensors are used to detect faults in pipelines (Kurmer *et al.* 1991). Phase signals induced by acoustic waves are detected by sensors and by using null frequency and output spectrum the leak locations are identified (Bhuiyan *et al.* 2016). Fiber optic sensors were used for detection of leakage in oil and gas pipelines using thermal monitoring due to their wide applicability (Qu *et al.* 2010). The results from this method proved its efficiency in detecting leak locations; however in the absence of soundproof material it could become inefficient (soundproof material has to be added to protect the sensing fiber from the surrounding noises). A support vector machine can be used to detect the defects in pipelines as proposed by Qu *et al.* (2010). Similar to the previous method, leak locations are detected by means of sensors which are attached to optical cables to sense the signals of vibrations. These signals are then transformed into electrical signals and then transmitted and processed by an analogue-to-digital converter. When a phase change of light waves occurs, the leakage along a pipeline can be detected. This method offers good performance and precision for identifying and locating leakage in pipelines, however the accuracy is linked to the amount of datasets gathered from the field. Piezoelectric sensors are used to identify the shortest wave paths generated from leakage in pipelines by combining the geometric boundaries using the local coordinate system (Grabec 1978; Ozevin & Harding 2012). This method considers the distance from leak locations to the sensor as the shortest wave path (Ozevin 2011). The waves are usually generated due to the flow turbulence inside pipelines as a result of leakage. The sensors detect these waves, from which the leak locations are identified. In this method locating time-dependent leakage in pipelines is possible; however the accuracy of the results in complex pipelines is questionable. Hu *et al.* (2011) investigated the applicability of the harmonic wavelet method for detecting leak locations in long pipelines. Precise identification of small leaks could be difficult because it requires noise cancellation in the background so as not to affect the accuracy of the obtained results. The harmonic wavelet method minimizes these errors because it can calculate the sudden drop in pressure waves and the time difference is analyzed showing the leak locations. Using the harmonic wavelet transform, the pressure signals are decomposed onto each wavelet level with the results shown in the form of time frequency maps. This approach is successful in detecting small leaks, however the process is somewhat lengthy.

Ground penetrating radar (GPR) has also been used for detecting leaks in buried water pipelines (Stampolidis *et al.* 2003; Nakhkash & Mahmood-Zadeh 2004; Takahashi &

Sato 2006; Ayala-Cabrera *et al.* 2011; Lai *et al.* 2016). Although it was considered as a reliable and effective method, it requires skilled operators and to some extent is costly, and in addition results obtained for metallic pipelines are not accurate. The acoustic technique is another technique being used for leak detections in water networks. In this technique, when water leaks from a pipe, noise is generated and propagated along the ground and the pipe. The acoustic technique translates this noise into actual numbers by connecting two ends of a pipe to sensors and measuring the delay in the sound signal detection at each end, hence locating the exact location of the leak (Gao *et al.* 2006; Mirats-Tur *et al.* 2014). In addition to being penetrative, slow and affected by external noises close to the pipe location, such as moving vehicles, the acoustic techniques are not applicable to all types of pipes (e.g. PVC) (Mirats-Tur *et al.* 2014). Moreover, large leaks do not generate detectable high frequency waves. Visual inspection by installing cameras inside the pipes is another leak detection technique that can produce visual evidence of the leak location. This process is considered to be invasive, where it involves a complete shutdown of the system (Hao *et al.* 2012).

In this study, a non-invasive method is proposed to detect and determine leak locations effectively and at the same time overcome limitations associated with currently utilized leak detection methods. A combined methodology of using GPR for accurate determination of pipe location, followed by an infrared (IR) thermography imaging technique for determining leak location is proposed. An IR thermography imaging technique was proposed for leak detection by Fahmy & Moselhi (2010), Carreño-Alvarado *et al.* (2014) and Al Hawari *et al.* (2015). The application of thermography using a thermal camera is considered a non-invasive technology that can be used to inspect and investigate buried infrastructures in a timely and cost-effective manner (Carreño-Alvarado *et al.* 2014). In this study, the IR thermography imaging technique was combined for the first time with GPR technology in order to obtain more accurate results. Moreover, the IR thermography imaging technique was also used for the first time in extreme, hot weather conditions rather than cold or moderate weather conditions. GPR sends electromagnetic waves through the ground to the subsurface and reflections from the objects underground are sent back to be received by the radar. The waves are emitted and received back through an antenna, creating a profile of the subsurface (Nakhkash & Mahmood-Zadeh 2004). Using this approach, GPR enables the detection of the buried pipes; thermographic imaging, on the other hand, was chosen to locate leaks since the imaging detects the temperature differences between surfaces. When a leak exists, the water-leaking location has a different temperature from its surroundings, hence showing a contrast in the images captured (Eyuboglu *et al.* 2003; Bimpas *et al.* 2010). The thermographic images were statistically analyzed using analysis of variance (ANOVA) and pairwise comparison methods in an attempt to accurately define the leak location. Two scenarios were studied in Doha, which were a simulated leak and an actual leakage case in real life. Different surfaces, environmental conditions and operating conditions were tested to confirm the applicability and flexibility of the approach in predicting leak locations.

METHODOLOGY

The proposed methodology is based on on-site experimental work from which data was collected using two scenarios, namely simulated leak and real leak. A combination of using both GPR to define the buried pipes locations and IR thermography to identify leak locations was used. The simulated scenario was performed in order to study the applicability of the proposed methodology under controlled conditions and predefined leaks. The real-case scenario, on the other hand, was performed in order to study the effect of altered conditions surrounding the pipe (emissivity and ambient temperature) on the results and to validate the applicability of the proposed methodology. In the setup for experimental work, different combinations for the height of the camera from the ground and the speed of camera were used as shown in Table 1. Once the images were collected by the IR camera the scale of each image was adjusted in order to obtain a strong color contrast. In the ANOVA analysis, which was performed using R-studio and Minitab commercial software packages, the mean temperature of each image was compared with the mean temperature of the whole set. Based on the test statistics that resulted

Table 1 | IR camera experimental operating conditions

Operating condition	Height from ground surface (m)	Speed (km/h)	Number of frames
1	1	2	1 (frame/second)
2	2	5	
3	1	5	
4	2	2	

from the ANOVA analysis enough evidence was obtained to reject or not to reject the null hypothesis. After the ANOVA analysis, pairwise comparison was carried out in order to identify the locations of the leak. A pairwise comparison between the mean temperatures of each image within the same set was performed using a Tukey procedure in Minitab and the differences were summed up for each image. In Tukey's procedure, the means are compared simultaneously for every operation and differences that are greater than the expected standard deviation are identified (Tukey 1949). The most suitable operating conditions of the IR camera in terms of detecting and locating water leaks were determined in all scenarios. Finally, a validation of the proposed methodology was done by comparing detected leak locations and the actual leak locations. The methodology of the study is described in Figure 1.

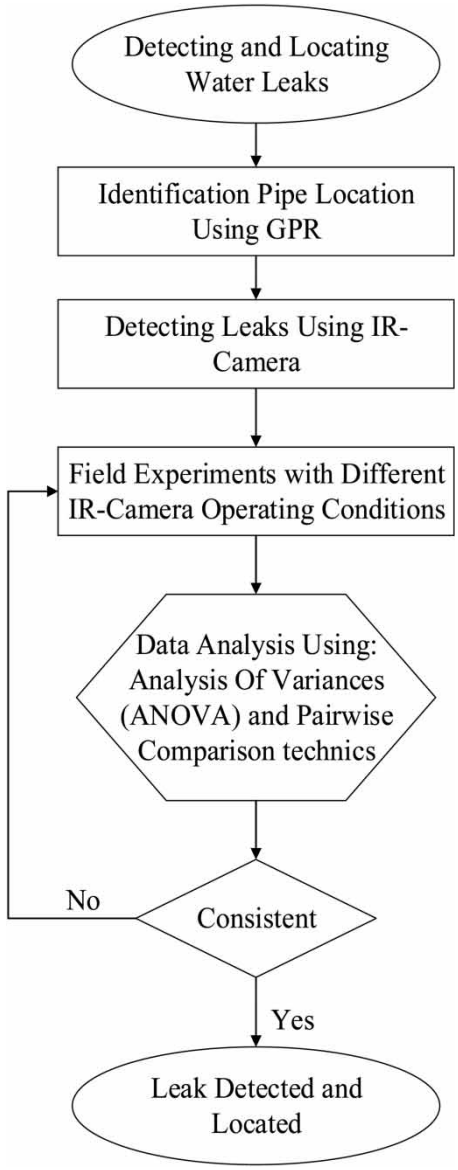

Figure 1 | Proposed methodology.

GPR system

GPR sends electromagnetic waves through the ground to the subsurface and then reflections from underground objects are received again by the radar. The waves are emitted and received back through an antenna, creating a profile of the subsurface. A MALÅ GPR, placed on a Terraplus Rough Terrain Cart (RTC), was used in this study. The MALÅ GPR was equipped with two shielded antennas, the 250 MHz antenna (dimensions: $0.74 \times 0.44 \times 0.16$ m; weight: 7.85 kg) and the shielded 500 MHz antenna (dimensions: $0.50 \times 0.30 \times 0.16$ m; weight: 5.0 kg). Antennas with lower frequency produce a higher wavelength and lower resolution images, but are able to detect objects that lie deep under the surface; on the other hand higher frequency antennas can detect shallower objects and will present higher resolution results (Eyuboglu *et al.* 2003). In this study both antennas were used in order to compare their efficiency and accuracy in locating the underground water pipes.

Thermography IR camera system

A VarioCAM hr head thermographic system was used in performing the set of field experiments, which has a long wave infrared spectral range (LWIR) of 7.5 to 14 μm. The lens reflects the object scene onto a

Table 2 | Technical specifications of VarioCAM hr head system

Spectral range	7.5 to 14 μm
Temperature measuring range	(−40 to 1,200) °C
Emissivity	Adjustable from 0.1 to 1.0 in increments of 0.01
Recording, image format (pixels)	384 × 288
Spectral range	Long wave infrared spectral range (LWIR) of 7.5 to 14 μm
Standard lens (FOV)	1.0/25 mm (30 × 23)° at (384 × 288)
IR frame rate	50/60 Hz
Zoom function	Up to 8 digital, infinitely variable
Operation temperature	(−15 to 50) °C
Storage temperature	(−40 to 70) °C
Humidity during operation and storage	Relative humidity 5% to 95%, non-condensing
Dimensions (complete system)	(133 × 106 × 110) mm
Weight (complete system)	Approx. 1.3 kg
Automatic functions	auto focus, auto-image, auto-level, alarm

microbolometer array at a resolution of 384 × 288 pixels, which means that each image will be translated to 110,592 temperature data points. A wide-angle lens was used to capture the IR radiation emitted by the object in the field of view (FOV) and to duplicate it onto the detector array with a focal length of 12.5 mm and a minimum focus of 0.2 m. Other properties and technical specifications of the VarioCAM hr system are shown in Table 2.

CASE STUDIES

Simulated leak scenario

In the first phase of the study, a leak from a 1 inch (2.5 cm) diameter PVC pipe was simulated under specific controlled conditions in order to verify the applicability of the proposed methodology. The pipe was 16.5 m long and was buried at 0.9 m depth surrounded by clayey soil. The leak was simulated by wetting a specific location along the length of the pipe. The wetted location had a wetted area with a radius of around 50 cm (Figure 2). The temperature of the water used in the simulated leak was 23 °C, while the ground surface and the ambient air temperatures were 35 °C and 32 °C, respectively. The relative humidity was 55%. The GPR was utilized to accurately identify the location of pipes under the surface

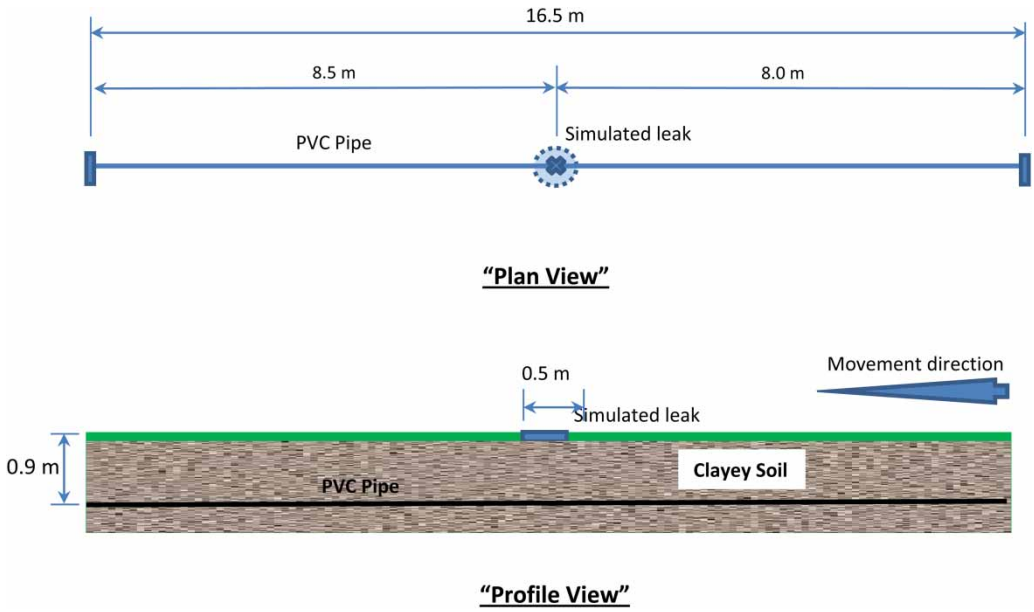

Figure 2 | Simulated leak experimental layout.

by moving in a specific path where it had to intercept perpendicularly with the expected location of the pipe at several points as shown in Figure 3(a). The location of the pipe is indicated by the hyperbola as shown in Figure 3(b). After defining the exact location of the pipe, thermographic images of the ground surface above the pipeline were taken under the different studied operating conditions. Four sets of images, corresponding to four different operating conditions, were collected.

Real leak scenario

In collaboration with Qatar General Electricity and Water Corporation (KAHRAMAA), a 7 metre long PVC pipe, buried 0.9 m under the surface and surrounded by crushed sandstone and brick pavement, was tested. According to KAHRAMAA, the pipeline was experiencing a leak, but the exact location of the leak was unknown. Thermographic images of the ground surface above the pipeline were taken under the different operating conditions. Four sets of images corresponding to each operating condition were collected. After collecting the images, the exact leak location was determined by KAHRAMAA through excavation and visual inspection. The temperature of the dry surface varied between 47 and 50 °C; meanwhile, the ambient air temperature and the relative humidity were 42 °C and 75%, respectively.

RESULTS AND DISCUSSION

IR-camera setup

After collecting the IR images, their scale was adjusted to obtain a strong color contrast. As shown in Figure 4(a) the color degradation for the simulated leak ranged from pink (37 °C), representing the highest temperature, to blue, representing the lowest temperature (26 °C). Since the temperature of the water used to simulate the leak (i.e. 24 °C) was less than the surrounding ground surface temperature, the orange color in Figure 4(b) would represent the leak. Figure 4(c) shows that in the case of the real leak, the color degradation was minimal with the color being mainly dark blue. Meanwhile, Figure 4(d) represents the location of the leak in the real leak case, in which a degradation in color can be observed. The temperature of water on the surface due to the real leak (i.e. 51–53 °C) was higher than the surrounding ground surface temperature (i.e. 47–50 °C).

ANOVA and pairwise comparison

Four different IR camera operating conditions were analyzed in which each operating condition was repeated twice and the averaged data were recorded. The thermographic images from each run were collected along the pipe length. The existence of a leak throughout the whole set of images was considered to be a function of the mean

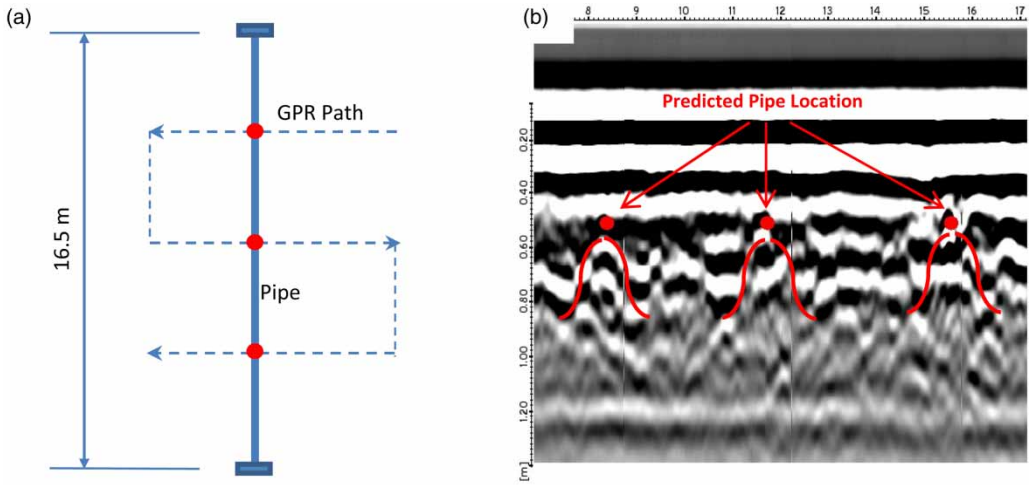

Figure 3 | (a) Path of the GPR on top of the buried pipe; (b) profile of the subsurface using the MALÅ ground penetrating radar (GPR) equipped with the 500 MHz shielded antenna, location of the pipe is indicated by the hyperbola and by the red dots. Please refer to the online version of this paper to see this figure in color: http://dx.doi.org/10.2166/ws.2017.044.

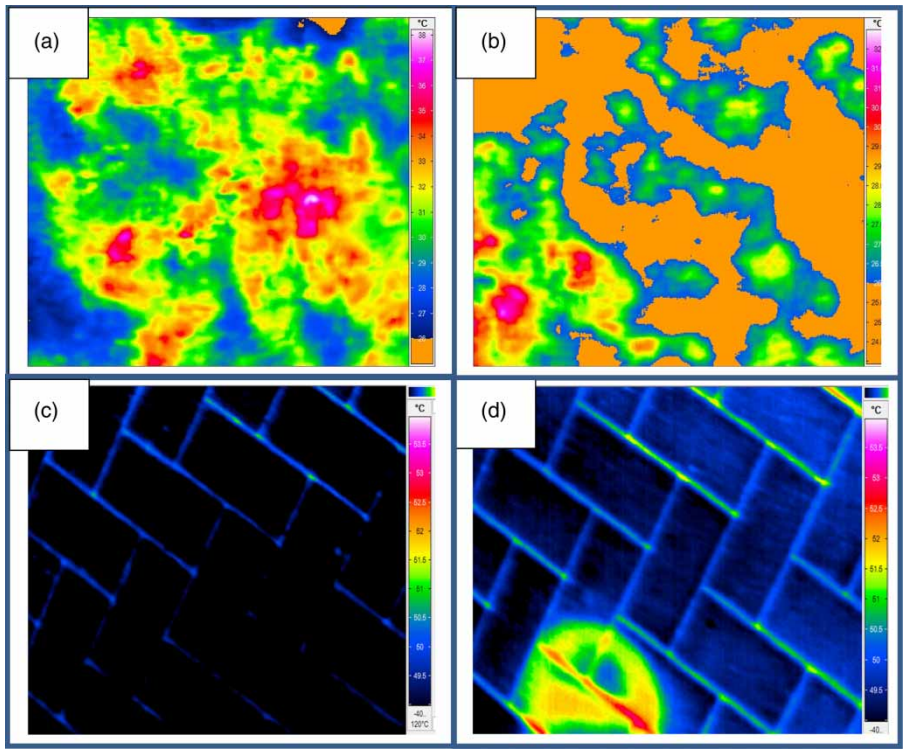

Figure 4 | (a) IR image for simulated leak case study 'dry location'; (b) IR image for simulated leak case study 'wet location'; (c) IR image for real leak case study 'dry location'; (d) IR image for real leak case study 'wet location'.

temperature differences between images of the same set. An ANOVA was performed for each set of the IR images for every operating condition. In the ANOVA analysis, the temperature of each image was compared with the mean temperature of each image in the whole set. If the null hypothesis (H_o: equal mean temperatures throughout ($\mu_1 = \mu_2 = \ldots = \mu_n$ where n is the number of thermographic images in a set)) is rejected this could be an indication of a leak existing. The failure to reject the null hypothesis means that equal mean temperatures exist which indicates that no leak is present and no temperature contrast will be recorded. Based on the test statistics resulting from ANOVA, F-values and probability values (p-value) were determined and compared with 0.05 as a significance level (α). A p-value of less than 0.05 indicates enough evidence to reject the null hypothesis H_o.

Simulated and real leak analysis

As mentioned earlier four sets of tests were performed along the pipeline (one set of images for each operating condition). Temperature values from the collected images were then statistically analyzed using ANOVA. It can be seen from Table 3 that in the case of the simulated and the real leak the resulting F-values were very high and the associated p-values were less than the specified significance level ($\alpha = 0.05$). This gives enough evidence to reject the null hypothesis (H_o) under all operating conditions, which means that a temperature contrast does exist among the collected data sets.

Table 3 | Test statistics for the simulated and real leak scenarios for the four operating conditions

Scenario	Operating condition	F-value	*p*-value
Simulated leak	1	1,024.00	0.00
	2	366.80	0.00
	3	523.30	0.00
	4	806.90	0.00
Real leak	1	103,240.00	0.00
	2	13,494.10	0.00
	3	77,780.80	0.00
	4	21,142.04	0.00

Consequently pairwise comparison between the mean temperatures of each image within the same set was performed using a Tukey procedure in Minitab and the differences were summed up for each image. An illustration of such an analysis is shown in Table 4 for operating condition (1) in the simulated leak case. The same process was repeated for all the operating conditions in the simulated and real leak cases. The outcomes of the ANOVA and pairwise comparison for the simulated leak and the real leak are graphically summarized in Figures 5 and 6, respectively. As shown in Figure 5, in the case of the simulated leak, operating condition (1) (camera height 1 m and camera speed 2 km/h) had the best prediction results followed by operating condition (4) (camera height 2 m and camera speed 2 km/h). The reason behind this could be due to the high variation in the recorded temperature contrast with respect to distance, which indicates that a leak is present in the locations having these high variations. As for the real leak, the best prediction results were obtained under operating conditions (2) and (3) (condition (2): 1 m height and camera speed 5 km/h, and condition (3): 2 m height and camera speed 5 km/h). The best prediction results were determined according to two factors: firstly the ability to predict the existence of a leak and secondly the ability to locate the leak. For the first factor, in all cases (simulated and real leaks) and under all running conditions the ANOVA analysis gave enough evidence to reject the null hypothesis (p-value less than $\alpha = 0.05$), which indicated the existence of a leak. For the prediction of the location of the leak, from the pairwise comparison results it was found that several factors had an impact on the enhancement of the thermal contrast and therefore affected the prediction of the location of the leak. The factors that were taken into consideration in this study were categorized into three main categories: characteristics of the studied surface (emissivity), characteristics of the surrounding environment (ambient temperature and relative humidity), and the operating conditions of the IR camera (speed and height from the surface).

Impact of the characteristics of the studied surface (emissivity)

The emissivity of the surface is very important as it defines how much thermal energy an object of interest can radiate; rougher and darker surfaces have the highest emissivity (Ozevin 2011). It was found that the captured thermal contrast depends on the characteristics of the surface emitting the energy. In the case of the simulated leak, the surface was a low emissivity surface (clayey soil ($\varepsilon = 0.39$)), while in the real leak case the surface was highly emissive (bricks ($\varepsilon = 0.93$)). A slower speed of the IR camera was required for low emissivity surfaces in order for the camera to be able to capture the thermal contrast at the real leak location. Therefore, in this case at a higher speed of 5 km/h the IR camera could not capture the exact location of the thermal contrast (Figure 5(b) and 5(c)). In the case of the highly emissive surface (i.e. bricks) at lower speed the IR camera could not capture the thermal contrast at the location of the leak. The predicted leak location at the two studied heights of the camera was shifted almost the same distance away from the real leak location in the direction of movement as shown in Figure 6(a) and 6(d). This could be due to the fact that the real leak case was performed in the summer at high ambient temperature (42 °C) and high relative humidity (75%).

Impact of the characteristics of the surrounding environment (ambient temperature and relative humidity)

It is anticipated that high ambient temperature and high relative humidity would also create contrasts in the IR thermography process. Thus, the accuracy of the readings in IR thermography would be affected. Consequently, on summer days with high humidity, lower IR detection ranges would be expected than in conditions with low humidity (Zachar & Naik 1992; Beier & Gemperlein 2004; Marinetti & Cesaratto 2012). It was found in this study that under high ambient temperature and relative humidity conditions the higher speed of the IR camera would reduce the impact of such side factors (noise) on the thermal contrast and therefore would give better results in predicting the location of the leak as shown in Figure 6(b) and 6(c).

Impact of the operating conditions of the IR camera (speed and height from the surface)

It was found that in the simulated leak case (low ambient temperature, low relative humidity and low emissivity

Table 4 | Pairwise comparison results for simulated leak with operating condition (1) (camera height of 1 m and camera speed of 2 km/h)

Images	1	2	3	4	5	6	7	8	9	10	11	12	13	14	15
1	0	0.049	1.295	1.397	1.051	0.223	0.169	0.554	1.55	0.913	0.28	1.655	1.273	0.927	0.914
2	0.049	0	1.246	1.348	1.561	0.173	0.177	0.505	1.501	0.864	0.225	1.406	1.004	0.878	0.865
3	1.295	1.246	0	0.102	0.313	0.927	0.873	1.259	0.255	0.618	0.985	0.659	0.0223	0.368	1.618
4	1.397	1.348	0.102	0	0.211	0.826	0.772	1.157	0.153	0.516	0.883	0.258	0.124	0.471	1.517
5	1.051	1.561	0.313	0.211	0	0.614	0.561	0.946	0.0586	0.304	0.671	0.246	0.646	0.65	1.305
6	0.223	0.173	0.927	0.826	0.614	0	0.122	1.331	1.673	1.311	0.575	0.768	0.951	1.301	0.891
7	0.169	0.177	0.873	0.772	0.561	0.122	0	2.385	2.619	2.256	2.111	3.011	2.869	3.242	1.745
8	0.554	0.505	1.259	1.157	0.946	1.331	2.385	0	1.004	1.641	1.274	1.899	2.281	2.627	2.021
9	1.55	1.501	0.255	0.153	0.0586	1.673	2.619	1.004	0	2.363	2.731	2.105	1.552	1.623	1.363
10	0.913	0.864	0.618	0.516	0.304	1.311	2.256	1.641	2.363	0	0.367	0.258	0.641	0.986	1.001
11	0.28	0.225	0.985	0.883	0.671	0.575	2.111	1.274	2.731	0.367	0	0.127	0.645	0.353	0.214
12	1.655	1.406	0.659	0.258	0.246	0.768	3.011	1.899	2.105	0.258	0.127	0	0.065	0.121	0.0122
13	1.273	1.004	0.0223	0.124	0.646	0.951	2.869	2.281	1.552	0.641	0.645	0.065	0	0.0212	0.058
14	0.927	0.878	0.368	0.471	0.65	1.301	3.242	2.627	1.623	0.986	0.353	0.121	0.0212	0	0.054
15	0.914	0.865	1.618	1.517	1.305	0.891	1.745	2.021	1.363	1.001	0.214	0.0122	0.058	0.054	0
Σ	**12.25**	**11.802**	**10.5403**	**9.735**	**9.1376**	**11.686**	**22.912**	**20.884**	**20.5506**	**14.039**	**11.441**	**12.5902**	**12.1525**	**13.6222**	**13.5782**

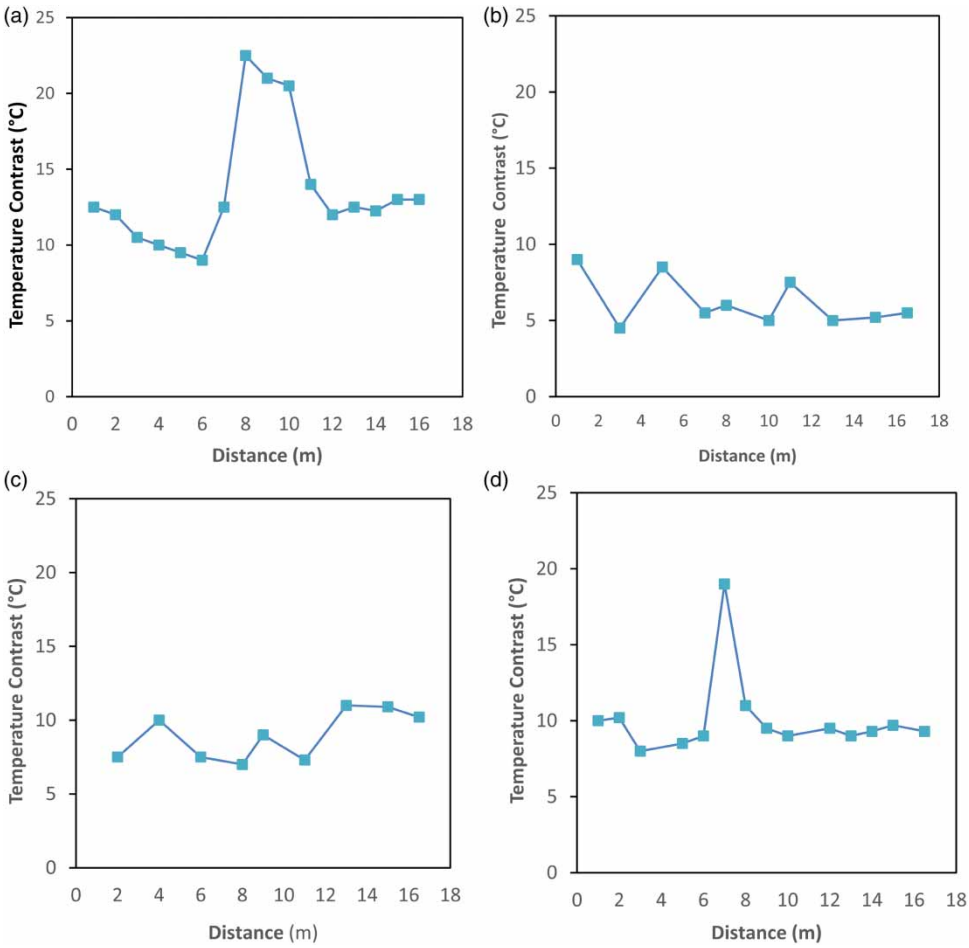

Figure 5 | (a) Predicted leak locations of the simulated leak case, operating conditions (1); (b) predicted leak locations of the simulated leak case, operating conditions (2); (c) predicted leak locations of the simulated leak case, operating conditions (3); (d) predicted leak locations of the simulated leak case, operating conditions (4).

surface) the lower speed of the camera gave better results in identifying the location of the leak than the higher camera speed (Figure 5(a) and 5(d)), whereas in the real leak case (high ambient temperature, high relative humidity and highly emissive surface), better results were obtained when the speed of the camera was higher (Figure 6(b) and 6(c)). Furthermore, in the case of the simulated leak, the height of camera had a direct impact on the enhancement of the thermal contrast compared to the real leak case. It was found that at a lower height of the camera, better leak predictions were obtained. However, the height of the camera had minimal impact on enhancing the captured thermal contrasts in the real leak case. The height of the camera from the surface would affect the FOV of the camera. The FOV of the camera used was 1.0/25 mm $(30 \times 23)^{\circ}$ at (384×288), which translates to a FOV of 0.34 m × 0.45 m at a 1 m distance with a 1.2 mm pixel, and 0.68 m × 0.90 m at a distance of 2 m with a 2.4 mm pixel. Therefore, at lower heights less area is covered per frame which means a more homogenous temperature distribution per frame. Consequently, the contrast between the different frames will be higher. The error of leak location prediction was calculated for both case studies by comparing the difference of distances between the beginning and the end of the actual leak location with the beginning and the end of the predicted leak location. Table 5 summarizes the error of prediction in the simulated and real leak cases under the four different operating conditions.

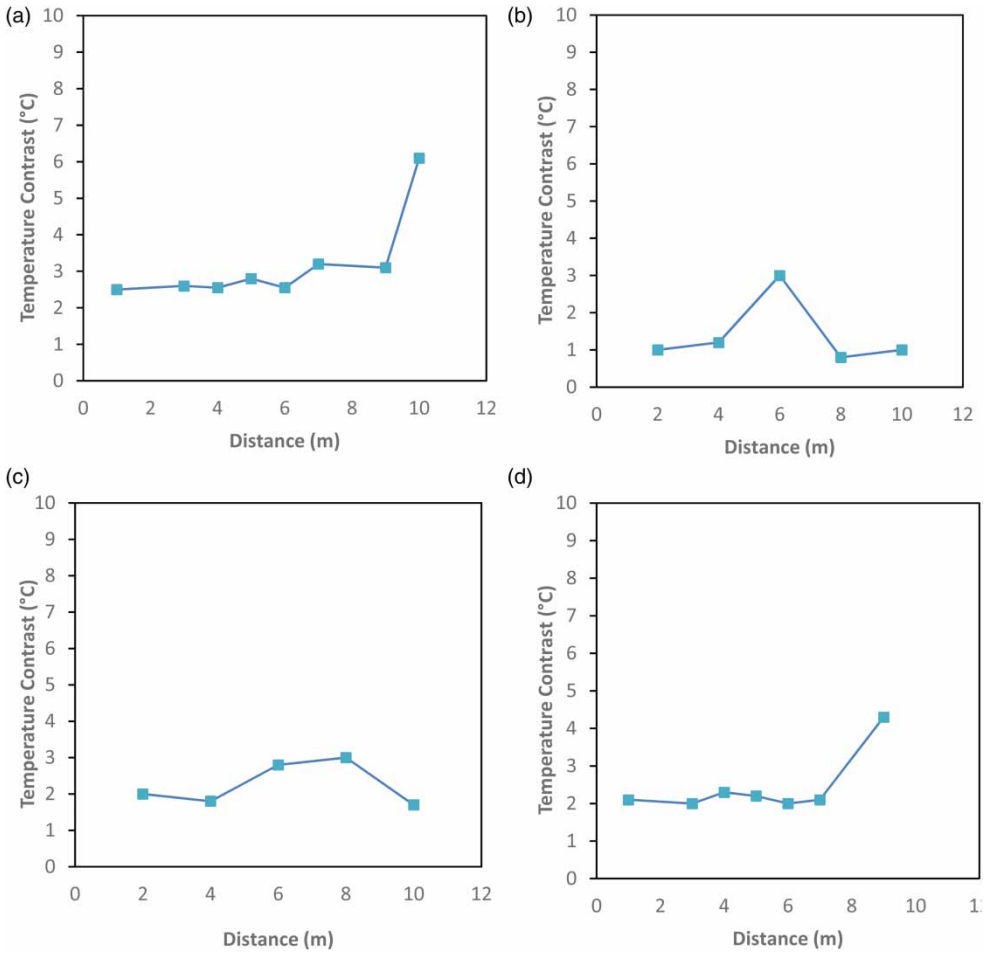

Figure 6 | (a) Predicted leak locations of the real leak case, operating conditions (1); (b) predicted leak locations of the real leak case, operating conditions (2); (c) predicted leak locations of the real leak case, operating conditions (3); (d) predicted leak locations of the real leak case, operating conditions (4).

Table 5 | Error measurements for the simulated and the real leak scenarios

Operating condition	1	2	3	4
Simulated leak location	Leak: 8.0–8.5 m			
Predicted leak boundaries	6.6–9.9 m	Not detected	1.8–3.7 m	5.9–7.1 m
Error %[a]	0%	Not detected	33.4%	11%
Real leak location	Leak: 6.0 m			
Predicted leak boundaries	8.8–10.0 m	4.0–6.0 m	4.0–8.0 m	7.5–8.8 m
Error%[a]	33.8%	10%	0%	21.3%

[a]Error calculation for leak $= \frac{\text{leak (measured)} - \text{average location of the predicted leak}}{\text{pipe length}}$.

CONCLUSIONS

In this study a new non-destructive methodology has been proposed in order to detect and determine leak locations effectively in WDNs. A combined methodology using GPR to accurately locate pipes, followed by thermographic technology to predict the leak location, was tested. The IR thermographic images were statistically analyzed using

ANOVA and pairwise comparison methods. Two case scenarios were studied; one with a simulated leak and the other with a real-life leak. Several factors were found to affect the accuracy of the proposed methodology in predicting the leak location, namely the characteristics of the studied surface (i.e. emissivity), the characteristics of the surrounding environment (i.e. ambient temperature and relative humidity), and the operating conditions of the IR camera (i.e. speed and height of the camera). In the case of low emissivity surfaces a slower camera speed would be required in order for the camera to be able to capture the thermal contrast at the real leak location. The results obtained in this study have also shown that under high ambient temperatures and high relative humidity conditions, a higher speed of the IR camera would reduce the impact of noise on the collected thermal contrast and therefore would give better leak location prediction results. The FOV is affected by the camera's height from the surface. At lower heights, less area will be covered per frame; therefore, a more homogenous temperature distribution per frame will be obtained. Consequently, the contrast between the different frames will be higher and better leak predictions will be expected.

The tested methodology proved the flexibility of the approach and the ability of accurately predicting the leak locations under different conditions. However, the main limitation of using IR thermography for leak prediction in water networks is that the leak should reach the upper surface close to the ground surface in order for the camera to be able to capture the thermal contrast. Otherwise no thermal contrast will be captured. Future studies should consider using GPR for leak prediction coupled with IR thermography, as well as performing the same experimental setup under different controlled operating conditions while observing the different outputs for each condition.

ACKNOWLEDGEMENTS

This publication was made possible by NPRP grant # (NPRP-5-165-2-055) from the Qatar National Research Fund (a member of The Qatar Foundation). The statements made herein are solely the responsibility of the authors. The authors would also like to acknowledge the Qatar General Electricity and Water Corporation (KAHRAMAA) for their cooperation and help.

REFERENCES

Al Hawari, A., Khader, M., Zayed, T. & Moselhi, O. 2015 Non-destructive visual-statistical approach to detect leaks in water mains. *International Journal of Environmental, Chemical, Ecological, Geological and Geophysical Engineering* **9**, 225–229.

Alkasseh, J. M. A., Adlan, M. N., Abustan, I., Aziz, H. A. & Hanif, A. B. M. 2013 Applying minimum night flow to estimate water loss using statistical modeling: a case study in Kinta Valley, Malaysia. *Water Resour. Manage.* **27**, 1439–1455.

Ayala-Cabrera, D., Herrera, M., Izquierdo, J. & Pérez-García, R. 2011 Location of buried plastic pipes using multi-agent support based on GPR images. *J. Appl. Geophys* **75** (4), 679–686.

Beier, K. & Gemperlein, H. 2004 Simulation of infrared detection range at fog conditions for enhanced vision systems in civil aviation. *Aerospace Science and Technology* **8**, 63–71.

Bhuiyan, M. A. S., Hossain, M. A. & Alam, J. M. 2016 A computational model of thermal monitoring at a leakage in pipelines. *Int. J. Heat Mass Transf.* **92**, 330–338.

Bimpas, M., Amditis, A. & Uzunoglu, N. 2010 Detection of water leaks in supply pipes using continuous wave sensor operating at 2.45 GHz. *Journal of Applied Geophysics* **70**, 226–236.

Carreño-Alvarado, E. P., Ayala-Cabrera, D., Pérez-García, R. & Izquierdo, J. 2014 Identification of buried pipes using thermal images and data mining. *Procedia Engineering*, **89**, 1445–1451 (16th Water Distribution System Analysis Conference, WDSA2014: Urban Water Hydroinformatics and Strategic Planning).

Cataldo, A., Persico, R., Leucci, G., De Benedetto, E., Cannazza, G., Matera, L. & De Giorgi, L. 2014 Time domain reflectometry, ground penetrating radar and electrical resistivity tomography: a comparative analysis of alternative approaches for leak detection in underground pipes. *NDT & E International* **62**, 14–28.

Eyuboglu, S., Mahdi, H. & Al-Shukri, H. 2003 Detection of water leaks using ground penetrating radar (GPR). In: *Proceedings of the Third International Conference on Applied Geophysics*, *Orlando, FL*, December 8–12.

Fahmy, M. & Moselhi, O. 2010 Automated detection and location of leaks in water mains using infrared photography. *Journal of Performance of Constructed Facilities* **24**, 242–248.

Gao, Y., Brennan, M. J. & Joseph, P. F. 2006 A comparison of time delay estimators for the detection of leak noise signals in plastic water distribution pipes. *Journal of Sound and Vibration* **292**, 552–570.

Ge, C., Wang, G. & Ye, H. 2008 Analysis of the smallest detectable leakage flow rate of negative pressure wave-based leak

detection systems for liquid pipelines. *Comput. Chem. Eng.* **32**, 1669–1680.

Grabec, I. 1978 Application of correlation techniques for localization of acoustic emission sources. *Ultrasonics* **16** (3), 111–115.

Hao, T., Rogers, C. D. F., Metje, N., Chapman, D. N., Muggleton, J. M., Foo, K. Y., Wang, P., Pennock, S. R., Atkins, P. R., Swingler, S. G., Parker, J., Costello, S. B., Burrow, M. P. N., Anspach, J. H., Armitage, R. J., Cohn, A. G., Goddard, K., Lewin, P. L., Orlando, G., Redfern, M. A., Royal, A. C. D. & Saul, A. J. 2012 Condition assessment of the buried utility service infrastructure. *Tunn. Undergr. Space Technol.* **28**, 331–344.

Hu, J., Zhang, L. & Liang, W. 2011 Detection of small leakage from long transportation pipeline with complex noise. *J. Loss Prev. Process Industries* **24**, 449–457.

Huang, S., Lin, W.-W., Tsai, M. & Chen, M. 2007 Fiber optic in-line distributed sensor for detection and localization of the pipeline leaks. *Sensors Actuators A* **135**, 570–579.

Ishido, Y. & Takahashi, S. A. 2014 New indicator for real-time leak detection in water distribution networks: design and simulation validation. *Procedia Engineering* **89**, 411–417.

Kingdom, B., Liemberger, R. & Marin, P. 2006 *The Challenge of Reducing Non-Revenue Water (NRW) in Developing Countries*. Water Supply and Sanitation Board Discussion Paper Series 8, The International Bank for Reconstruction and Development, The World Bank, Washington, DC, USA.

Kurmer, J. P., Kingsley, S. A., Laudo, J. S. & Kark, S. J. 1991 Distributed fiber optic acoustic sensor for leak detection. In: *Distributed Multiplexed Fiber Optic Sensors*, SPIE Proceedings 1586, SPIE, Bellingham, WA, USA, pp. 117–128.

Lai, W. W. L., Chang, R. K. W., Sham, J. F. C. & Pang, K. 2016 Perturbation mapping of water leak in buried water pipes via laboratory validation experiments with high-frequency ground penetrating radar (GPR). *Tunn. Undergr. Space Technol.* **52**, 157–167.

Marinetti, S. & Cesaratto, P. G. 2012 Emissivity estimation for accurate quantitative thermography. *NDT & E International* **51**, 127–134.

Mirats-Tur, J. M., Jarrige, P.-A., Meseguer, J. & Cembrano, G. 2014 Leak detection and localization using models: field results. *Procedia Engineering* **70**, 1157–1165.

Nakhkash, M. & Mahmood-Zadeh, M. 2004 Water leak detection using ground penetrating radar. In: *Proceedings of the Tenth International Conference on Ground Penetrating Radar, Delft, The Netherlands*, June 21–24, IEEE, Piscataway, NJ, USA, pp. 525–528.

Ozevin, D. 2011 Geometry-based acoustic source location for spaced structures. *Int. J. Struct. Health Monit.* **10** (5), 503–510.

Ozevin, D. & Harding, J. 2012 Novel leak localization in pressurized pipeline networks using acoustic emission and geometric connectivity. *Int. J. Press. Vessels Pip.* **92**, 63–69.

Qu, Z., Feng, H., Zeng, Z., Zhuge, J. & Jin, S. 2010 A SVM-based pipeline leakage detection and pre-warning system. *Measurement* **43**, 513–519.

Stampolidis, A., Soupios, P., Vallianatos, F. & Tsokas, G. N. 2003 Detection of leaks in buried plastic water distribution pipes in urban places – a case study. In: *Proceedings of the 2nd International Workshop on Advanced Ground Penetrating Radar, Delft, The Netherlands*, IEEE, Piscataway, NJ, USA, pp. 120–124.

Sun, L. & Chang, N. 2014 Integrated-signal-based leak location method for liquid pipelines. *J. Loss Prev. Process Industries* **32**, 311–318.

Takahashi, K. & Sato, M. 2006 A novel inversion of cross-hole radar data for location of buried pipes. In: *Proceedings of the 11th International Conference on Ground Penetrating Radar*, IEEE, Piscataway, NJ, USA.

Tukey, J. W. 1949 Comparing individual means in the analysis of variance. *Biometrics* **5** (2), 99–114.

Xu, Q., Liu, R., Chen, Q. & Li, R. 2014 Review on water leakage control in distribution networks and the associated environmental benefits. *Journal of Environmental Sciences* **26**, 955–961.

Zachar, J. & Naik, T. 1992 Principles of infrared thermography and application for assessment of the deterioration of the bridge deck at the Zoo Interchange. In: *Process and Materials Engineering Congress*, ASCE, New York, USA, pp. 107–115.

Zangenehmadar, Z. & Moselhi, O. 2014 Study of leak detection technologies in water distribution networks. In: *General Conference 2014 de la SCGC*, 28–31 May, Halifax, Canada.

First received 19 December 2016; accepted in revised form 29 March 2017. Available online 11 April 2017